

Long-distance wireless power transfer system powering multiple loads with constant voltage outputs using S-SP compensation

ISSN 1755-4535

Received on 16th August 2019

Revised 10th December 2019

Accepted on 25th February 2020

doi: 10.1049/iet-pel.2019.0880

www.ietdl.org

Chenwen Cheng¹, Zhe Zhou², Weiguo Li², Jianghua Lu¹, Zhanfeng Deng², Chunting Chris Mi¹ ✉

¹Department of Electrical and Computer Engineering, San Diego State University, 5500 Campanile Drive, San Diego, CA, USA

²State Key Laboratory of Advanced Power Transmission Technology (Global Energy Interconnection Research Institute), Changping District, Beijing 102211, People's Republic of China

✉ E-mail: mi@ieee.org

Abstract: This paper proposes a long-distance multi-load wireless power transfer (WPT) system with a constant voltage (CV) output for each load. A repeater unit consisting of two bipolar repeater coils is designed to power the load. Multiple repeater units are placed in a line and the power can be transferred from one unit to the next. Each repeater unit corresponds to one load and multiple loads can be powered simultaneously. The two repeater coils in the same repeater unit are placed perpendicularly to eliminate the magnetic coupling between them. In each repeater unit, a compensation capacitor is placed in series with the transmitting coil while two extra compensation capacitors form a series-parallel (SP) structure for the receiving coil. When neglecting the coil's parasitic resistance, the CV characteristics can be obtained, which enables the independent and flexible power control of each load. Moreover, the influence of the parasitic resistances on the system performance is analysed. Such a system is especially suitable for powering the gate drivers in a high-voltage converter where multiple insulated gate bipolar transistors (IGBTs) are connected in series. An experimental setup with six loads is constructed to validate the proposed system. The maximum system efficiency can reach 88.1%.

1 Introduction

Multiple isolated power supplies are necessary for the gate drivers in the series-connected insulated gate bipolar transistors in a high-voltage converter because their reference potentials are different [1]. The wireless power transfer (WPT) technology provides an ideal solution for powering the multiple gate drivers with enough insulation level because no direct contact is needed [2, 3]. In addition, the system using the proposed WPT technology is independent of the main power. Thus, the gate driver can be powered before the power-on of the main power and can still work during a power outage, which ensures operation safety. However, only one load can be powered in the conventional WPT system [4–9], which cannot meet the multiple load requirements in the gate driver application.

Powering multiple loads using WPT technology is attracting more and more attention recently [10–15]. In [10], the frequency bifurcation phenomenon was used to transfer power to multiple loads where each receiver works at a specific bifurcation frequency. However, the load number is limited by the number of split frequencies. A multi-load WPT system was proposed in [11] to power the LEDs where the transmitting coil is compensated using the LCC topology and multiple loads are connected in parallel across the unique receiving coil. The multiple receivers, however, are not isolated and are not suitable for the gate driver application. In [12], the game-theory-based control strategy was developed for load power control. However, the magnetic coupling between different receiving coils is not considered. A WPT system with multiple outputs was developed for charging the electric vehicles in [13]. Multiple transmitting coils are connected in parallel across the inverter, each of which corresponds to a receiving coil. In order to suppress the magnetic coupling between an adjacent pair of coils, these coils should be placed with enough space between them. In [14, 15], the repeater coils were adopted to power multiple loads over a long distance. The constant current (CC) can be obtained for all loads, which greatly suppressed the load power coupling and simplified the load power control. However, the constant voltage (CV) source is preferred in the gate driver application. Thus, an extra conversion circuit like the LCL circuit should be used to transform the CC source to CV source

before they are used to power the gate drivers, which will increase the system cost and loss.

In order to generate a CV output for the load, the S-SP compensation topology with one load was proposed in [16, 17] where one capacitor is connected in series with the transmitting coil and two capacitors are connected to the receiving coil to form a series-parallel (SP) circuit. The series-connected capacitors resonate with the leakage inductance while the parallel-connected capacitor resonates with the magnetising inductance to eliminate reactive power. In this paper, the S-SP topology is adopted and extended to the multi-load application. The repeater coils [14, 15, 18] are used in the proposed system. Every two repeater coils form a repeater unit and each repeater unit corresponds to one load. One repeater coil in the repeater unit receives power from its previous unit while the other repeater coil transmits power to its subsequent unit. Moreover, the bipolar coils are adopted for all the repeater coils. The two bipolar repeater coils in the same repeater unit are placed perpendicularly so that the magnetic coupling between them can be eliminated [19]. The S-SP compensation topology is implemented in each repeater unit. An experimental setup with six loads is constructed to validate the effectiveness of the proposed multi-load WPT system.

The main contributions of this paper are listed below:

- (i) In the proposed WPT system, multiple isolated CV outputs can be generated with a simple system structure, which is suitable for powering gate drivers where isolated voltage sources are required;
- (ii) The S-SP compensation topology is adopted in the proposed system. This is the first time that the S-SP compensation topology is applied in a multi-load WPT system, the working principle of which is analysed;
- (iii) Detailed analysis of the proposed WPT system using the S-SP compensation method is conducted, which shows that the load voltages decrease gradually as the load power increases when considering the coil's resistance. To obtain a better CV characteristic and higher system efficiency, a larger coupling coefficient or quality factor is required.

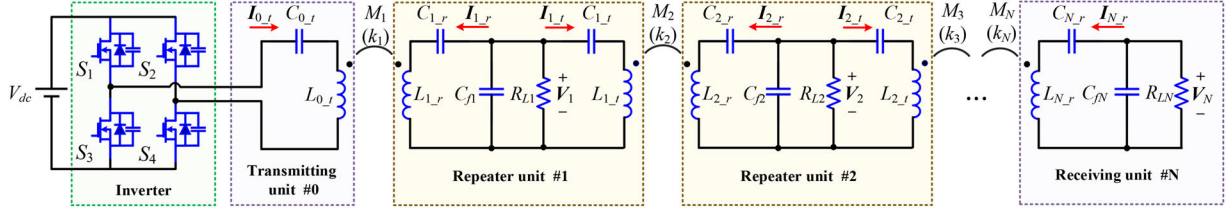


Fig. 1 Topology structure of the proposed WPT system

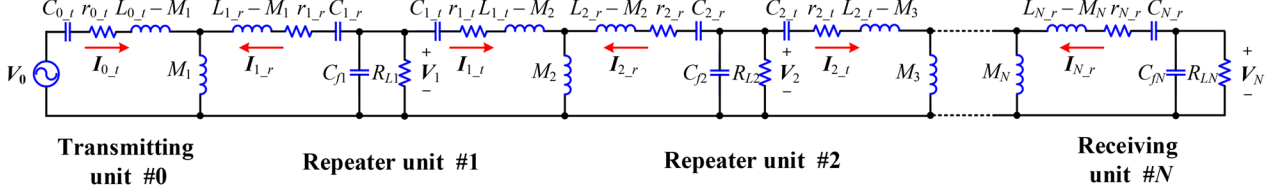


Fig. 2 Equivalent circuit model of the proposed WPT system

2 System description

2.1 System modelling

Fig. 1 shows the topology structure of the proposed WPT system with N loads, which is divided into three groups, i.e. the transmitting unit #0, repeater unit #1 ($1 \sim N-1$) and receiving unit # N . Each repeater unit # n ($n = 1, 2, \dots, N-1$) and the receiving unit # N corresponds to a load. In each repeater unit, there are two repeater coils. The receiving coil $L_{n,r}$ receives power from its previous unit while the transmitting coil $L_{n,t}$ transmits power to the next unit ($n = 1, 2, \dots, N-1$). There are three compensation capacitors, namely $C_{n,r}$, C_{fn} and $C_{n,t}$ in the repeater unit # n ($n = 1, 2, \dots, N-1$), which forms a series (S) compensation for $L_{n,t}$ and a series-parallel (SP) compensation for $L_{n,r}$. An H-bridge inverter consisting of four metal-oxide-semiconductor field-effect transistors (MOSFETs) is used to generate a high-frequency AC voltage from the DC voltage V_{dc} for the repeater system, which is connected to the transmitting coil $L_{0,t}$ via the series-connected compensation capacitor $C_{0,t}$ in the transmitting unit #0. For receiving unit # N , only the receiving coil $L_{N,r}$ is needed together with the compensation capacitors $C_{N,r}$ and C_{fN} because it does not transmit power to any other unit. The load is connected in parallel with the compensation capacitor C_{fn} in the repeater unit or the receiving unit. Usually, a rectifier consisting of four diodes is adopted to transform the high-frequency AC power into a DC source for real applications. Since the voltage across the rectifier and the current flowing into the rectifier are in phase, the rectifier together with DC load can be modelled as an AC load R_{Ln} ($n = 1, 2, \dots, N$) [20]. Although there are many coils in the proposed system, only the magnetic coupling between $L_{n-1,t}$ and $L_{n,r}$ ($n = 1, 2, \dots, N$) needs to be considered as shown in Fig. 1 with the coil structure designed in Section 2.3. The mutual inductance and the corresponding coupling coefficient between $L_{n-1,t}$ and $L_{n,r}$ is defined as M_n and k_n ($n = 1, 2, \dots, N$), which have the following relationship:

$$k_n = \frac{M_n}{\sqrt{L_{n-1,t} \cdot L_{n,r}}} \quad (1)$$

2.2 Constant voltage outputs

The T-type model of two coupled inductors is adopted to analyse the proposed system as shown in Fig. 2. V_0 is the AC voltage source generated by the inverter. $r_{n,r}$ and $r_{n,t}$ are the parasitic resistances of $L_{n,r}$ and $L_{n,t}$, respectively. $I_{n,r}$ and $I_{n,t}$ are the currents flowing through $L_{n,r}$ and $L_{n,t}$, respectively ($n = 0, 1, 2, \dots, N$); V_n ($n = 1, 2, \dots, N$) is the load voltage across R_{Ln} . The positive directions of these currents or voltages are defined in Fig. 2. The voltage equations for all the loops in Fig. 2 can be written in (2) according to the Kirchhoff's voltage law

$$\begin{bmatrix} V_0 \\ V_1 \\ V_1 \\ V_2 \\ \dots \\ V_N \end{bmatrix} = \begin{bmatrix} Z_{0,t}j\omega_0 M_1 00 \dots 0 \\ j\omega_0 M_1 Z_{1,t} 00 \dots 0 \\ 00 Z_{1,t} j\omega_0 M_2 \dots 0 \\ 00 j\omega_0 M_1 Z_{2,r} \dots 0 \\ \dots \\ 0000 \dots Z_{N,r} \end{bmatrix} \cdot \begin{bmatrix} I_{0,t} \\ I_{1,t} \\ I_{1,r} \\ I_{2,t} \\ \dots \\ I_{N,r} \end{bmatrix} \quad (2)$$

where $Z_i = r_i + 1/(j\omega_0 C_i) + j\omega_0 L_i$, and i indicates the coil number and ω_0 is the operational angular frequency.

In the proposed WPT system, the following resonant condition should be met:

$$\omega_0^2 = \frac{1}{(L_{n-1,t} - M_n) \cdot C_{n-1,t}} = \frac{1}{(L_{n,r} - M_n) \cdot C_{n,r}} = \frac{1}{(M_n \cdot C_{fn})}, \quad n = 1, 2, \dots, N \quad (3)$$

The resonant condition in (3) means that the parallel-compensated capacitor C_{fn} should resonate with the mutual inductance M_n while the series-compensated capacitors $C_{n-1,t}$ and $C_{n,r}$ should resonate with the equivalent inductances $(L_{n-1,t} - M_n)$ and $(L_{n,r} - M_n)$, respectively, in the T-model. Substituting (3) into (2), the following equation can be obtained:

$$V_n = V_{n-1} - r_{n-1,t} \cdot I_{n-1,t} + r_{n,r} \cdot I_{n,r}, \quad n = 1, 2, \dots, N \quad (4)$$

In an idealised case, the coil's parasitic resistance is very small so that it can be neglected. Thus, (4) can be simplified as

$$V_0 = V_1 = V_2 = V_3 = \dots = V_N \quad (5)$$

It can be seen from (5) that the amplitudes of the load voltages are constant regardless of the load resistance when neglecting the coil's parasitic resistance. When one load power varies, the other load voltage will not be affected, which means independent load power control can be achieved. The effect of the parasitic resistance on the CV operation will be discussed later in Section 3.

Fig. 3 shows the simulation waveforms of the load voltages using the proposed WPT system with six loads. The simulation is conducted in LTspice and the figure is redrawn using MATLAB. The simulation parameters are listed in Table 1 and the parasitic resistance is neglected. It can be seen that all load voltages have the same amplitude and phase.

2.3 Coil structure

The above analysis and the constant load voltage conclusion are based on the assumption that only the magnetic coupling between $L_{n-1,t}$ and $L_{n,r}$ ($n = 1, 2, \dots, N$) is considered while the coupling

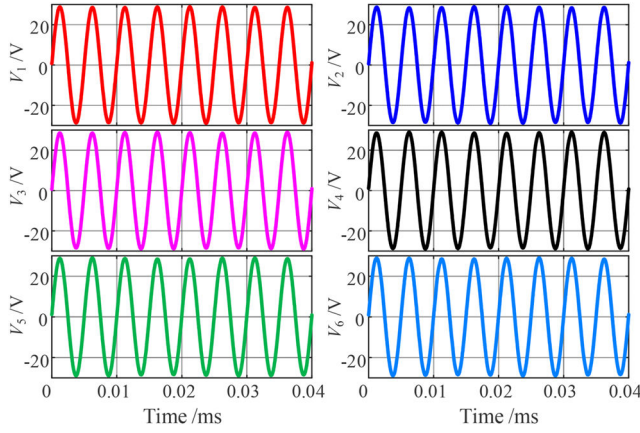


Fig. 3 Simulation waveforms of the proposed WPT system with six loads

Table 1 System parameters

Parameter	Value	Parameter	Value
V_{dc}	25 V	f_s	200 kHz
$L_{0_t} - L_{6_r}$	93 μ H	$C_{f1} - C_{f6}$	28.4 nF
$C_{0_t} - C_{5_t}$	8.96 nF	$C_{1_r} - C_{6_r}$	8.96 nF
k	0.24	Q	320

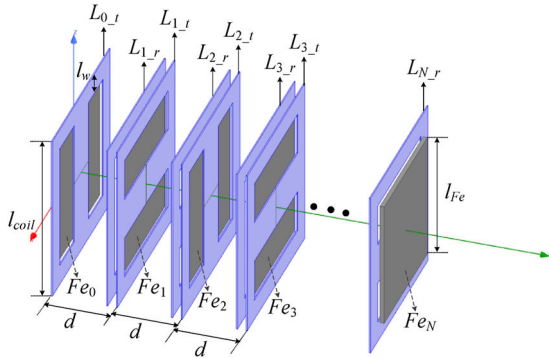


Fig. 4 Coil structure used in the proposed WPT system

Table 2 Simulated coupling coefficients

k_{1r_1t}	k_{1r_2r}	k_{1r_2t}	k_2
0.0001	0.0001	0.0064	0.257

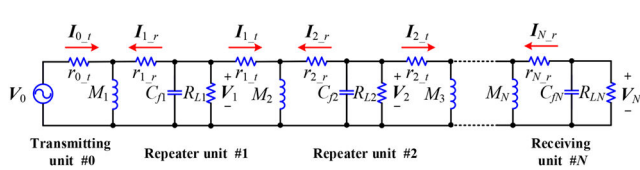


Fig. 5 Simplified circuit model considering the parasitic resistance

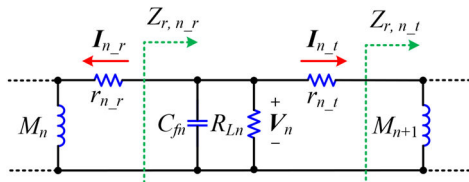


Fig. 6 Reflection impedances in the repeater unit #n

between any other two coils can be neglected. In order to achieve this goal, the coil structure proposed in [14, 15] is adopted in this paper as shown in Fig. 4, which will be described briefly.

To save space, the two repeater coils in the same repeater unit should be close. However, the magnetic coupling between them is undesirable. In order to eliminate the magnetic coupling between

them, the bipolar coils are used for both repeater coils. Moreover, the two bipolar coils are placed perpendicularly as seen in Fig. 4. As a result, their magnetic fields are orthogonal and the coupling between them is zero [19]. The ferrite plate Fe_n ($n = 0, 1, 2, \dots, N$) is inserted in each unit, which not only increases the magnetic coupling between L_{n-1_t} and L_{n_r} ($n = 1, 2, \dots, N$) but also suppresses that between any two non-adjacent coils.

The finite-element analysis is used to help design the coils. Considering the symmetric structure in Fig. 4, only repeater units #1 and #2 are simulated. The coils and ferrite plates are square with the side length of $l_{coil} = 160$ mm and $l_{Fe} = 120$ mm, respectively. The coil width is $l_w = 20$ mm. The distance between two adjacent units is $d = 60$ mm. The simulated coupling coefficients are listed in Table 2 where k_{1r_1t} , k_{1r_2r} , k_{1r_2t} , k_2 are the coupling coefficients between L_{1_r} and L_{1_t} , L_{1_r} and L_{2_r} , L_{1_r} and L_{2_t} , L_{1_t} and L_{2_r} , respectively. It can be seen from Table 2 that the other coupling coefficients are much smaller compared to k_2 , which can be neglected.

3 Detailed analysis

It should be pointed out that the CV characteristics of the loads are obtained in the proposed WPT system under the premise that the coils' parasitic resistances can be neglected. In practical applications, the coil' parasitic resistance is inevitable, the influence of which on the system performance is analysed below.

The quality factors of L_{n_t} and L_{n_r} are defined as Q_{n_t} and Q_{n_r} . Then their parasitic resistance r_{n_t} and r_{n_r} can be calculated as

$$r_{n_t} = \frac{\omega_0 L_{n_t}}{Q_{n_t}}, \quad r_{n_r} = \frac{\omega_0 L_{n_r}}{Q_{n_r}} \quad (6)$$

According to the resonant condition in (3), the circuit model shown in Fig. 2 can be simplified as in Fig. 5. It is really complicated to get the analytical solutions of the load voltages directly from Fig. 5 when the load number N is large because there are too many parallel- and series-connected circuits in Fig. 5. In this section, the reflection impedances in each coil are defined, then the recursive formulas of the reflection impedances and the load voltages can be derived. With the help of MATLAB, the load voltages can be easily obtained based on these recursive formulas.

Fig. 6 illustrates the reflection impedances in the two repeater coils in the repeater unit #n where $Z_{r,n,r}$ and $Z_{r,n,t}$ are the reflection impedances in $L_{n,r}$ and $L_{n,t}$, respectively. According to Fig. 6, $Z_{r,n,r}$ and $Z_{r,n,t}$ can be calculated as

$$\begin{cases} Z_{r,n,t} = \frac{j\omega_0 M_{n+1} \cdot (r_{n+1,r} + Z_{r,n+1,r})}{j\omega_0 M_{n+1} + r_{n+1,r} + Z_{r,n+1,r}} \\ Z_{r,n,r} = \frac{R_{Ln}(r_{n,t} + Z_{r,n,t})}{R_{Ln} + (r_{n,t} + Z_{r,n,t}) \cdot (j\omega_0 C_{fn} R_{Ln} + 1)} \end{cases} \quad (7)$$

In the receiving unit #N, the reflection impedance $Z_{r,N,r}$ can be calculated by (8) because there is no transmitting coil

$$Z_{r,N,r} = \frac{R_{LN}}{(j\omega_0 C_{fN} R_{LN} + 1)} \quad (8)$$

The reflection impedance $Z_{r,0,t}$ in the transmitting unit #0 can also be calculated using (7). Thus, the reflection impedance in each coil can be calculated one by one iteratively from the last coil, $L_{N,r}$, to the first coil, $L_{0,t}$.

3.1 Load voltage

Once all the reflection impedances are obtained, the currents flowing through the coils and the load voltages in repeater unit #n can be calculated as

$$\begin{cases} I_{n,r} = -\frac{(V_{n-1} - I_{n-1,l} \cdot r_{n-1,l})}{(r_{n,r} + Z_{r,n,r})} \\ V_L = V_{n-1} - I_{n-1,l} \cdot r_{n-1,l} + I_{n,r} \cdot r_{n,l,r} \\ I_{n,l} = \frac{V_n}{(r_{n,l} + Z_{r,n,l})} \end{cases} \quad (9)$$

Using (9), the load voltages can be calculated iteratively beginning with transmitting unit #0. The load voltage variations against the increasing load power are shown in Fig. 7. According to the coil structure in Section 2.3, the quality factors and the parasitic resistances of all the repeater coils are identical, i.e.

$$\begin{cases} L_{0,l} = L_{1,r} = L_{1,l} = L_{2,r} = \dots = L_{N,r} = L \\ Q_{0,l} = Q_{1,r} = Q_{1,l} = Q_{2,r} = \dots = Q_{N,r} = Q \\ r_{0,l} = r_{1,r} = r_{1,l} = r_{2,r} = \dots = r_{N,r} = r \end{cases} \quad (10)$$

In Fig. 7, there are six loads where $k=0.24$, $Q=320$. These parameters are consistent with those in the experimental prototype in Section 4. However, the analysis method and conclusion are applicable to other parameters. In order to facilitate the comparison, the load voltage and load power are normalised by dividing the base values defined as

$$V_b = V_0, \quad R_b = \omega_0 M, \quad P_b = \frac{V_b^2}{R_b} \quad (11)$$

It needs to be pointed out that the selection of R_b does not affect the analysis. Moreover, the load resistances R_{Ln} ($n=1, 2, \dots, N$) are assumed identical in Fig. 7, i.e.

$$R_{L1} = R_{L2} = \dots = R_{LN} = R_L \quad (12)$$

It needs to be pointed out that this assumption is not a necessary condition for the proposed system, which is used here just to facilitate the comparison. Moreover, the identical load resistance ensures nearly equal power distribution among all the loads. In a practical case, the proposed system with different load resistances can still work well, which will be shown in the experimental part in Section 4.

Assuming that the load voltage variation is small, the normalised load power can be calculated as

$$P_{Ln_norm} = \frac{P_{Ln}}{P_b} = \left(\frac{V_n^2}{R_L} \right) / \left(\frac{V_b^2}{R_b} \right) \approx \frac{R_b}{R_L} \quad (13)$$

Thus, the x -axis in Fig. 7 is R_b/R_L , which roughly equals the normalised load power. In Fig. 7, the load voltages decrease gradually as the load power increases. Moreover, the load voltage decreases faster if the unit is further from transmitting unit #0.

In order to study the influence of the coupling coefficient k and quality factor Q on the CV performance, Fig. 8 shows the variation of the last load voltage V_6 with different k and Q where there are six loads and $R_b/R_L=0.2$. If V_6/V_b is closer to 1, better CV characteristics can be obtained for the proposed system. According to Fig. 8, with a larger k or Q , a larger load voltage V_6 can be obtained, which indicates a better CV performance. In an ideal case where the coil's resistance is zero, which means Q is infinite, the voltage drop is zero. Thus, an ideal CV source can be obtained. However, in a practical application, the load voltage drop cannot be avoided because the coil's resistance is inevitable.

3.2 Input impedance angle

The input impedance angle of the whole system to the inverter is also shown in Fig. 9. When considering the parasitic resistance, the input impedance is a little inductive. As can be seen from Fig. 9, the input impedance angle is less than 5° , which changes slightly with the increasing load power. Thus, only a little amount of reactive power is generated in the proposed system. Moreover, the

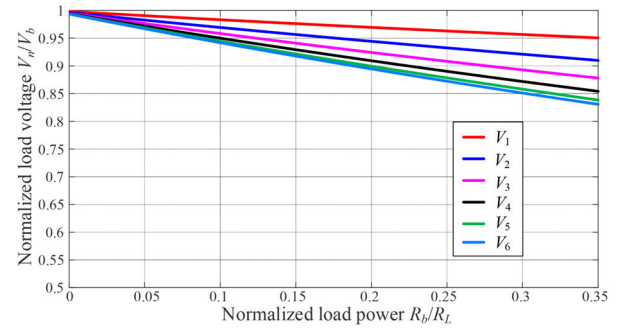


Fig. 7 Load voltage variations versus the increasing load power considering the coil's parasitic resistances ($N=6$, $k=0.24$, $Q=320$)

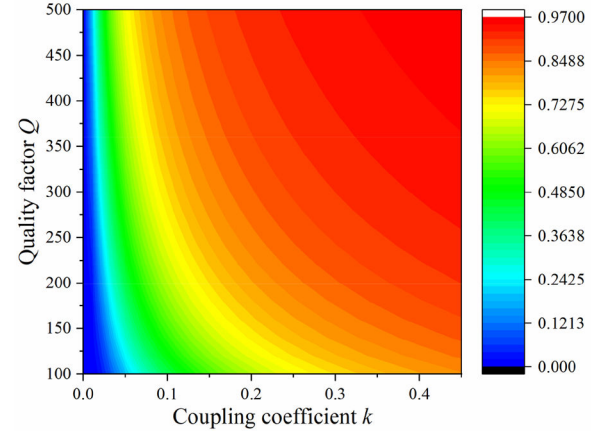


Fig. 8 Variation of the last load voltage with different coupling coefficients k and quality factors Q ($N=6$, $R_b/R_L=0.2$)

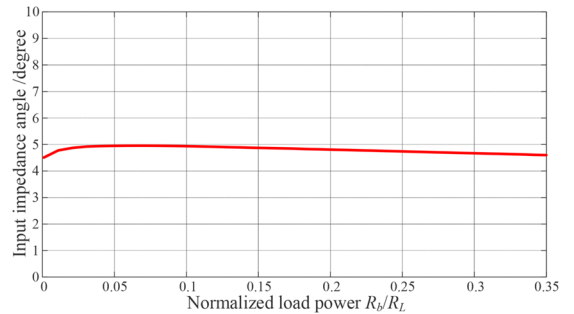


Fig. 9 Input impedance angle with the increasing load power ($N=6$, $k=0.24$, $Q=320$)

small inductive input impedance facilitates the zero voltage switching of the MOSFETs in the inverter [21]. Thus, the switching loss can be decreased.

3.3 System efficiency

The AC to AC efficiency can also be calculated with the load voltage V_n obtained in (9) as

$$\eta = \sum_{n=1}^N \left(\frac{V_n^2}{R_{Ln}} \right) / \text{Re}[V_0 \cdot I_{0,l}] \quad (14)$$

where $\text{Re}[X]$ represents the real part of X .

Fig. 10 shows the system efficiency variation with the increasing load power using (14) where $N=6$, $k=0.24$, $Q=320$. In this case, the maximum efficiency is about 85.6% when the normalised load power is about 0.19. The maximum achievable efficiency is affected by the coupling coefficient k and the quality factor Q . Fig. 11 shows the maximum achievable efficiency of the proposed WPT system with different k and Q . It can be seen that a larger k or Q is beneficial to improve the system efficiency. This

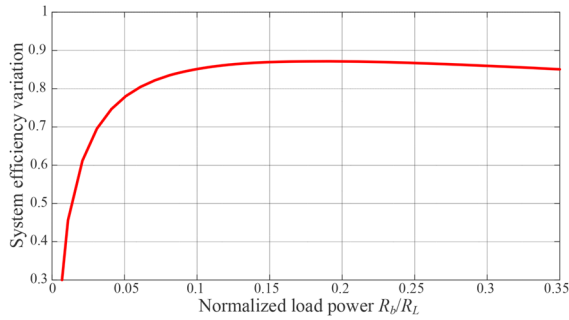


Fig. 10 System efficiency variation against the load power ($N = 6$, $k = 0.24$, $Q = 320$)

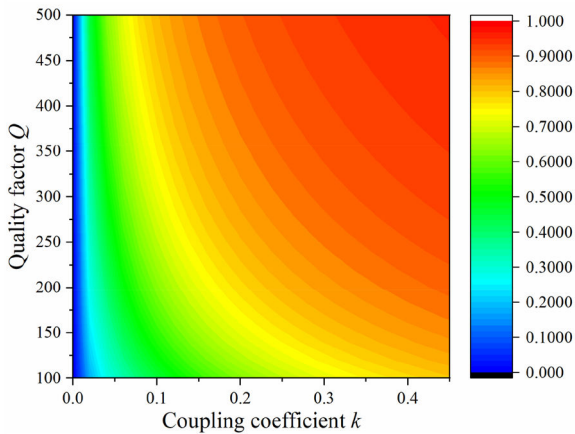


Fig. 11 Variation of the maximum achievable system efficiency with different coupling coefficients k and quality factors Q ($N = 6$)

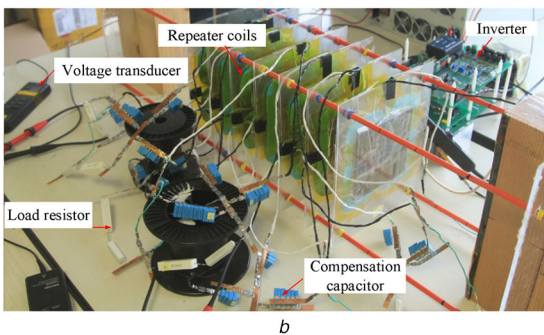
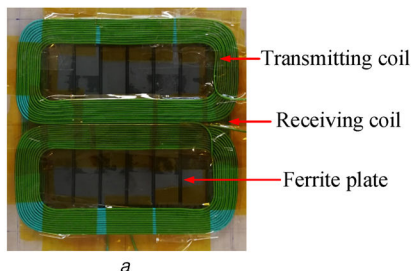


Fig. 12 Experimental setup with six loads
(a) Repeater unit, (b) Experimental platform

conclusion is similar to that in the conventional one-load WPT system.

4 Experimental validation

4.1 Experimental setup

The repeater unit and a WPT system with six loads was designed as shown in Figs. 12a and b, respectively, to validate the proposed WPT system. The 660-strand Litz wire is used to fabricate the coils, so that the skin-effect loss can be reduced, and the quality factor of the coil can be improved. The dimensions of the

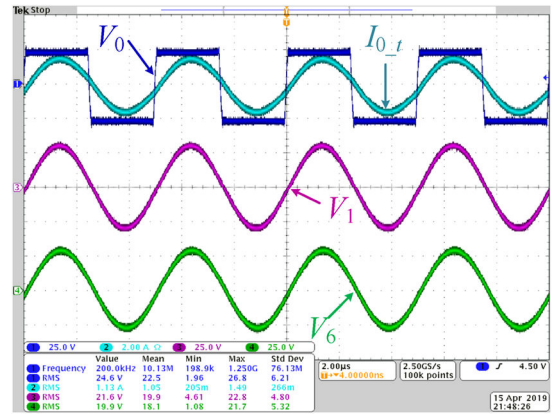


Fig. 13 Experimental waveforms

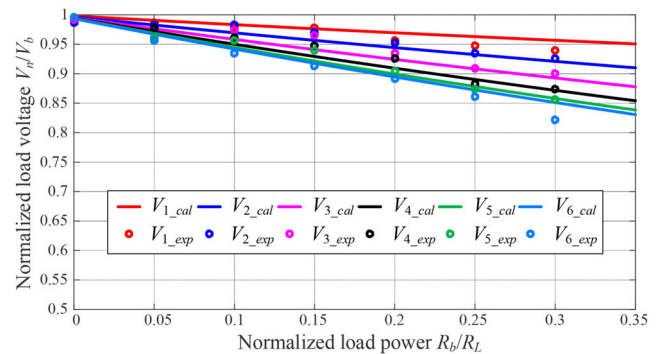


Fig. 14 Load voltage variation with the increasing load power

experimental setup are $l_{\text{coil}} = 160$ mm, $l_{\text{Fe}} = 120$ mm, $l_w = 20$ mm and $d = 60$ mm, which are consistent with the simulation parameters above. The coupling coefficient of two adjacent repeater units is 0.24. The quality factor of the coil is around 320. The switching frequency of the system is set to 200 kHz, which is realised by the inverter consisting of four silicon carbide MOSFETs. The detailed system parameters are listed in Table 1.

4.2 Experimental results

Fig. 13 shows the experimental waveforms of the designed multi-load WPT system. The inverter's output voltage V_0 is in phase with the current $I_{0,t}$ flowing through the transmitting coil $L_{0,t}$, which means the power factor of the experimental system is close to 1. The load voltages V_1 and V_6 are also shown in Fig. 13. They have almost the same amplitude value. Moreover, V_1 and V_6 are in phase, which is consistent with the analysis in (5).

The load voltage variation with the increasing load power is shown in Fig. 14 where all load resistances are the same. The solid lines represent the calculated load voltages while the dotted points are measured voltages in the experiment. Due to the coil's parasitic resistance, the load voltage decreases gradually as the load power increases but within an acceptable range. As can be seen in Fig. 14, the calculated voltages and the measured voltages match well. The voltage drop can be decreased with a larger k or Q as analysed above.

In the real application, a DC/DC converter can be used before the gate driver circuit. Thus, although there are load voltage drops in Fig. 14, the output voltage of the DC/DC converter can be maintained constant with a wide input range.

The system efficiency variation with the increasing load power is shown in Fig. 15 where the solid line and dotted points are the calculated efficiency and measured efficiency, respectively. The measured efficiency is a little larger than the calculated value, which is mainly due to the measurement errors of the quality factor Q of the coil, the load voltages and the non-linearity of the ferrite material. The maximum measured efficiency can reach 88.1% when the normalised load power is 0.2.

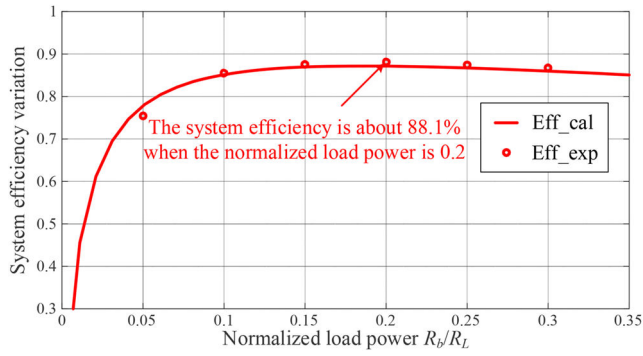


Fig. 15 System efficiency variation with increasing load power

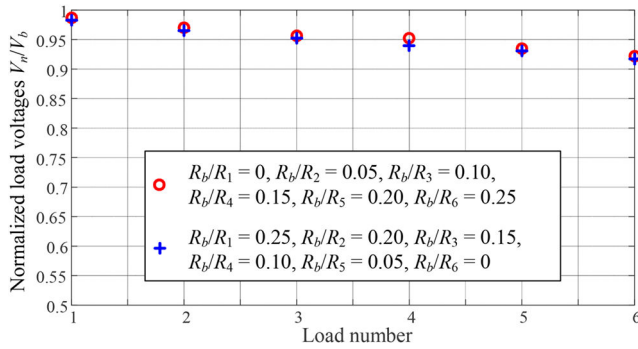


Fig. 16 Load voltage variations with different load resistances

Fig. 16 shows the load voltage variations with six different load resistances. The red circles represent the six load voltages where $R_b/R_1=0$, $R_b/R_2=0.05$, $R_b/R_3=0.10$, $R_b/R_4=0.15$, $R_b/R_5=0.20$, $R_b/R_6=0.25$ while the blue crosses represent the load voltages where $R_b/R_1=0.25$, $R_b/R_2=0.20$, $R_b/R_3=0.15$, $R_b/R_4=0.10$, $R_b/R_5=0.05$, $R_b/R_6=0$. Nearly constant load voltages can be obtained in both cases according to Fig. 16, which shows that the proposed WPT system functions well in different load conditions.

5 Conclusion

In this paper, a novel multi-load long-distance WPT system using S-SP compensation topology is designed. The repeater coils are used to enhance the power transfer capability over a long distance. The repeater unit that consists of two repeater coils is designed to power each load. Since the two repeater coils in the same repeater unit are placed perpendicularly, the magnetic coupling between them can be removed. With the S-SP compensation topology and the corresponding resonant condition, constant load voltages can be obtained for each load when neglecting the coils' parasitic resistances, which enables the independent and flexible power control of each load. The influence of coil parasitic resistances on the load voltages and system efficiency are also analysed, which shows that the load voltage-drop because of the parasitic resistances is within an acceptable range with a reasonable coupling coefficient and quality factor. An experimental setup with six loads has been designed and the experiment results validated the effectiveness of the proposed multi-load WPT system.

6 References

- [1] Rodriguez, J., Lai, J., Peng, F.Z.: 'Multilevel inverters: a survey of topologies, controls, and applications', *IEEE Trans. Ind. Electron.*, 2002, **49**, (4), pp. 724–738
- [2] Takasaki, M., Miura, Y., Ise, T.: 'Wireless power transfer system for gate power supplies of modular multilevel converters'. Proc. IEEE Int. Power Electron. Motion Control Conf. ECCE Asia, Hefei, People's Republic of China, May 2016, pp. 3183–3190
- [3] Kusaka, K., Kato, M., Orikawa, K., *et al.*: 'Galvanic isolation system for multiple gate drivers with inductive power transfer – drive of three-phase inverter'. Proc. IEEE ECCE, Montreal, QC, Canada, Sep. 2015, pp. 4525–4532
- [4] Zhang, W., Mi, C.C.: 'Compensation topologies of high-power wireless power transfer systems', *IEEE Trans. Veh. Technol.*, 2016, **65**, (6), pp. 4768–4778
- [5] Feng, H., Cai, T., Duan, S., *et al.*: 'A dual-side-detuned series-series compensated resonant converter for wide charging region in a wireless power transfer system', *IEEE Trans. Ind. Electron.*, 2018, **65**, (3), pp. 2177–2188
- [6] Li, X., Tang, C., Dai, X., *et al.*: 'An inductive and capacitive combined parallel transmission of power and data for wireless power transfer systems', *IEEE Trans. Power Electron.*, 2018, **33**, (6), pp. 4980–4991
- [7] Yao, Y., Wang, Y., Liu, X., *et al.*: 'A novel parameter tuning method for a double-sided LCL compensated WPT system with better comprehensive performance', *IEEE Trans. Power Electron.*, 2018, **33**, (10), pp. 8525–8536
- [8] Lu, F., Zhang, H., Hofmann, H., *et al.*: 'A dual-coupled LCC-compensated IPT system with a compact magnetic coupler', *IEEE Trans. Power Electron.*, 2018, **33**, (7), pp. 6391–6402
- [9] Zhang, H., Lu, F., Hofmann, H., *et al.*: 'A four-plate compact capacitive coupler design and LCL-compensated topology for capacitive power transfer in electric vehicle charging application', *IEEE Trans. Power Electron.*, 2016, **31**, (12), pp. 8541–8551
- [10] Narayanamoorthi, R., Vimala Juliet, A., Chokkalingam, C., *et al.*: 'Cross interference minimization and simultaneous wireless power transfer to multiple frequency loads using frequency bifurcation approach', *IEEE Trans. Power Electron.*, 2014, **34**, (11), pp. 10898–10909
- [11] Li, Y., Hu, J., Li, X., *et al.*: 'Analysis, design and experimental verification of a mixed high order compensations-based WPT system with constant current outputs for driving multistring LEDs', *IEEE Trans. Ind. Electron.*, 2020, **67**, (1), pp. 203–213
- [12] Yin, H., Fu, M., Liu, M., *et al.*: 'Autonomous power control in a reconfigurable 6.78-MHz multiple-receiver wireless charging system', *IEEE Trans. Ind. Electron.*, 2018, **65**, (8), pp. 6177–6187
- [13] Vu, B.V., Phan, V.T., Dahidah, M., *et al.*: 'Multiple output inductive charger for electric vehicles', *IEEE Trans. Power Electron.*, 2019, **34**, (8), pp. 7350–7368
- [14] Cheng, C., Lu, F., Zhou, Z., *et al.*: 'Load-independent wireless power transfer system for multiple loads over a long distance', *IEEE Trans. Power Electron.*, 2019, **34**, (9), pp. 9279–9288
- [15] Cheng, C., Zhou, Z., Li, W., *et al.*: 'A multi-load wireless power transfer system with series-parallel-series compensation', *IEEE Trans. Power Electron.*, 2019, **34**, (8), pp. 7126–7130
- [16] Hou, J., Chen, Q., Yan, K., *et al.*: 'Analysis and control of S/SP compensation contactless resonant converter with constant voltage gain'. Proc. IEEE Energy Convers. Congr. Exposit. (ECCE), Denver, CO, USA, September 2013, pp. 2552–2558
- [17] Yao, Y., Wang, Y., Liu, X., *et al.*: 'Analysis and design of an S/SP compensated IPT system to minimized output voltage fluctuations versus coupling coefficient and load variation', *IEEE Trans. Veh. Technol.*, 2018, **67**, (10), pp. 9262–9272
- [18] Zhong, W., Lee, C.K., Hui, S.Y.R.: 'General analysis on the use of tesla's resonators in domino forms for wireless power transfer', *IEEE Trans. Ind. Electron.*, 2013, **60**, (1), pp. 261–270
- [19] Kan, T., Lu, F., Nguyen, T.D., *et al.*: 'Integrated coil design for EV wireless charging systems using LCC compensation topology', *IEEE Trans. Power Electron.*, 2018, **33**, (11), pp. 9231–9241
- [20] Li, S., Mi, C.C.: 'Wireless power transfer for electric vehicle applications', *IEEE J. Emerg. Sel. Topics. Power Electron.*, 2015, **3**, (1), pp. 4–17
- [21] Jiang, Y., Wang, L., Wang, Y., *et al.*: 'Analysis, design, and implementation of accurate ZVS angle control for EV battery charging in wireless high-power transfer', *IEEE Trans. Ind. Electron.*, 2019, **66**, (5), pp. 4075–4085